



Homogeneous and Graded Ag Alloying in (Cu_{1-x}Ag_x)₂ZnSnSe₄ Solar Cells

Louis Grenet, Fabrice Emieux, Frédéric Roux

► To cite this version:

Louis Grenet, Fabrice Emieux, Frédéric Roux. Homogeneous and Graded Ag Alloying in (Cu_{1-x}Ag_x)₂ZnSnSe₄ Solar Cells. *physica status solidi (a)*, 2020, 217 (9), pp.2000040. 10.1002/pssa.202000040 . cea-02952497

HAL Id: cea-02952497

<https://cea.hal.science/cea-02952497>

Submitted on 29 Sep 2020

HAL is a multi-disciplinary open access archive for the deposit and dissemination of scientific research documents, whether they are published or not. The documents may come from teaching and research institutions in France or abroad, or from public or private research centers.

L'archive ouverte pluridisciplinaire **HAL**, est destinée au dépôt et à la diffusion de documents scientifiques de niveau recherche, publiés ou non, émanant des établissements d'enseignement et de recherche français ou étrangers, des laboratoires publics ou privés.

Homogeneous and Graded Ag Alloying in $(\text{Cu}_{1-x}\text{Ag}_x)_2\text{ZnSnSe}_4$ Solar Cells

Louis Grenet,* Fabrice Emieux, and Frédéric Roux

$\text{Cu}_2\text{ZnSn}(\text{S,Se})_4$ (CZTSSE)-based solar cell performances are limited by band tailing due to a large amount of Cu_{Zn} antisite defects. Partially replacing the Cu atoms by larger Ag ones can significantly reduce the prevalence of these defects, which are particularly detrimental close to the front interface. Herein, the possibility of synthesizing $(\text{Cu}_{1-x}\text{Ag}_x)_2\text{ZnSnSe}_4$ absorbers with various Ag contents by vacuum-based processes is demonstrated. Although the synthesis of high-quality materials is demonstrated, their use in thin film photovoltaic devices does not exhibit performance improvement compared with efficient pure CZTSSE-based solar cells. Moreover, the comparison with literature data reopens the debate of the beneficial effect of homogeneous Ag alloying in kesterite. On the contrary, a new method is proposed to fabricate graded $(\text{Cu}_{1-x}\text{Ag}_x)_2\text{ZnSnSe}_4$ absorbers with increased Ag content at the interfaces. The solar cells with graded absorbers exhibit better performances than the reference Ag-free ones. Particularly, improved current collection at the back contact and slight reduction of the front interface recombination are demonstrated.

1. Introduction

$\text{Cu}_2\text{ZnSn}(\text{S,Se})_4$ (CZTSSE) absorbers have attracted considerable attention in the past few years due to their favorable optoelectronic properties for thin film photovoltaic (PV) applications without using critical raw materials. However, the maximum power conversion efficiencies (PCEs) of kesterite-based solar cells are limited to 12.6%, which is far from the 23.4% achieved by the chalcopyrite-based ones.^[1] The main difference between this cousin technology lies in a much smaller open-circuit voltage (V_{OC}) for the CZTSSE-based solar cells. This V_{OC} deficit can be partially attributed to band tails in the kesterite absorber, which arises from a large amount of Cu_{Zn} antisites in the lattice.^[2] Replacing part of the Cu atoms by Ag has been proposed as a solution to significantly reduce band tails in the absorber and thus the V_{OC} deficit.^[3,4] The fabrication of graded $(\text{Cu}_{1-x}\text{Ag}_x)_2\text{ZnSn}(\text{S,Se})_4$ (CAZTSSE)

absorbers with increasing $[\text{Ag}]/([\text{Cu}]+[\text{Ag}])$ (ACA) ratio toward the front surface is claimed to be particularly beneficial for the PV properties.^[4]

Some recent studies have shown an improvement of the kesterite-based solar cell PV properties with the introduction of Ag in the lattice.^[5–13] In almost all cases, the CAZTSSE absorbers (containing both S and Se) have been fabricated with solution-based processes and show an optimum ACA ratio between 3% and 20%. In the studies by Yan et al. and Yang et al.,^[8,12] physical vapor deposition (PVD) methods have been used to fabricate pure sulfide CAZTS absorbers, whereas in the study by Gershon et al.,^[9] a pure selenide CAZTSe absorber synthesized by a chemical method exhibits a small PCE improvement for a 10% ACA ratio. Interestingly, ACA-graded CAZTSSE absorbers have been fabricated in the study by Qi et al.^[6] with significant

PCE improvement. This grading is made possible by the solution process used, which consists of spin-coating multilayered CAZTS precursors with different ACA ratios.

In this study, we aim at demonstrating the fabrication of CAZTSe (pure selenide) materials with homogeneous and graded ACA ratio in the depth of the absorber by PVD synthesis processes. It is first shown that PVD processes are able to produce high-quality homogeneous CAZTSe solid solution with ACA ratio varying from 5% to 50%. A novel method is presented as well to produce graded CAZTSe absorbers with ACA ratio increasing toward front and back interfaces. Both homogeneous and graded alloys are then used in solar cells. A very large scan of the synthesis conditions for CAZTSe absorbers does not show any performance improvement compared with efficient pure CZTSe-based solar cells and opens the debate on whether the beneficial effect of Ag is universal or linked to specific device optimization in previous studies. On the contrary, increasing Ag content at the back contact helps to collect the carrier generated deep in the absorber and tackle the back contact issue^[14] in kesterite devices.

2. Results and Discussion


2.1. Material Characterization

2.1.1. Homogeneous Ag Alloying

In this study, two strategies have been followed to improve kesterite device performances with Ag alloying. In this first part,

Dr. L. Grenet, F. Emieux, Dr. F. Roux
Université Grenoble Alpes
F-38000 Grenoble, France
E-mail: louis.grenet@cea.fr

Dr. L. Grenet, F. Emieux, Dr. F. Roux
CEA
LITEN
17, rue des Martyrs, F-38054 Cédex 09 Grenoble, France

 The ORCID identification number(s) for the author(s) of this article can be found under <https://doi.org/10.1002/pssa.202000040>.

DOI: 10.1002/pssa.202000040

CAZTSe absorbers with various but constant ACA ratios throughout the depth of the layer have been synthesized.

To achieve this goal, a Ag layer has been added to the Cu/Sn/Cu/Zn/Se stack of precursors. Different ACA ratios have been targeted (0%, 5%, 10%, 20%, and 50%) by adjusting the thicknesses of the Ag and the intermediate Cu layers. For the sake of simplicity, the Ag layer can be deposited either below or above the Cu/Sn/Cu/Zn stack. Both configurations have been tested but has neither performed significantly better when used in a solar cell, nor revealed a much better morphology by scanning electron microscopy (SEM). The Cu/Sn/Cu/Zn/Ag stack has been chosen in the whole study. It is claimed in different studies,^[7,15] that the process temperature has to be decreased with Ag content for the CAZTSe absorber synthesis, particularly because of morphology degradation at high temperatures and a high Ag content. However, in our case, the temperature optimization (in the 400–500 °C range) has only been made by comparing the PCEs of the Mo/CAZTSe/CdS/i-ZnO/ZnO:Al devices. Systematically, the highest temperature gives the best or similar performance for all ACA ratios in the absorber. All samples shown thereafter have thus been synthesized at 500 °C for 5 min.

Due to the limited energetic resolution of the X-ray fluorescence (XRF) set up (overlapping between the Sn L and Ag L transition peaks), energy dispersive X-ray spectrometry (EDX) has been used to measure the CAZTSe absorbers composition (Table 1). A comparison between values measured by EDX and XRF is given as well for the pure Ag 0%. EDX measurement uncertainty is much larger than the XRF one and much more sensitive to sample inhomogeneity (lateral and in depth) because of a

shorter integration time and a limited number of measurement points (two per sample). By comparison, 36 points mapping is systematically made by XRF on the CZTSe samples. ACA ratios measured in the layers slightly differ from the targeted values, but the denomination ACA 0%, ACA 5%, ACA 10%, ACA 20%, and ACA 50% is maintained in the following.

X-ray diffraction (XRD) diffractograms of the CAZTSe samples for different ACA ratios are shown in Figure 1a. All peaks related to the kesterite structure (PDF 04-010-6295) are visible for all CAZTSe absorbers along with the Mo (110) peak and a broad MoSe₂ contribution around 32°. It is noticeable that the kesterite peaks are shifted to lower angles with increasing Ag content (a larger lattice constant) due to the substitution of the Cu element by the larger Ag atoms. A zoom on the (112) peak (Figure 1b) reveals that the shape of the shifted peak is not modified by Ag incorporation, indicating a homogeneous solid solution in the layer. It is visible as well that the separation of the (204/220) and (312/116) peak increases with Ag content (Figure 1a). It is attributed to a decrease in the *c/a* ratio in the lattice when Ag replaces Cu.^[7] Finally, for the ACA 50% sample, the signature of a surface SnSe₂ secondary phase is visible at 14.4° (only the low-angle peak is clearly visible^[16]) and is systematically present even when lowering the Sn content in the absorber. Thus, the synthesis of a CAZTSe pure phase with ACA ≈50% is not successfully achieved (at lower Ag content, no evidence of secondary phases has been obtained but the presence of a unique CZTSe phase cannot be claimed only based on XRD analysis).

To confirm the homogeneous solid solution throughout the depth of the layer, elemental profiles have been measured with glow discharge optical emission spectroscopy (GDOES) (Figure 2). ACA ratios are depicted for all samples as a function of the sputtering time, which is translated into depth in the absorber. Cu, Se, and Mo profiles (of the ACA 10% sample) are shown as well for clarity. These profiles confirm that a perfectly homogenous (Cu and Ag) alloying occurs throughout the layer. The small ACA increase at the surface is probably an artifact effect due to the Cu signal drop. Indeed, the hatched area is not reliable as the modulus and phase of the plasma impedance matching are fast varying.

Figure 3 shows the SEM top views of the CAZTSe absorbers with different ACA ratios. All these absorbers have been

Table 1. Composition of the CAZTSe absorbers measured by EDX. The values in brackets for Ag 0% are the XRF measurements made on the same sample.

Sample	Cu + Ag [at%]	ACA [%]	Zn [at%]	Sn [at%]
ACA 0%	44.3 ± 1.2 (42.6)	0.0	29.8 ± 1.3 (29.6)	25.9 ± 1.3 (28.0)
ACA 5%	45.7 ± 1.1	5.9 ± 2.9	27.8 ± 1.3	26.5 ± 1.3
ACA 10%	46.0 ± 1.1	10.5 ± 2.4	29.9 ± 1.3	24.1 ± 1.4
ACA 20%	46.1 ± 1.1	20.4 ± 1.9	27.8 ± 1.3	26.0 ± 1.3
ACA 50%	44.6 ± 1.1	48.1 ± 1.5	28.9 ± 1.3	26.5 ± 1.3

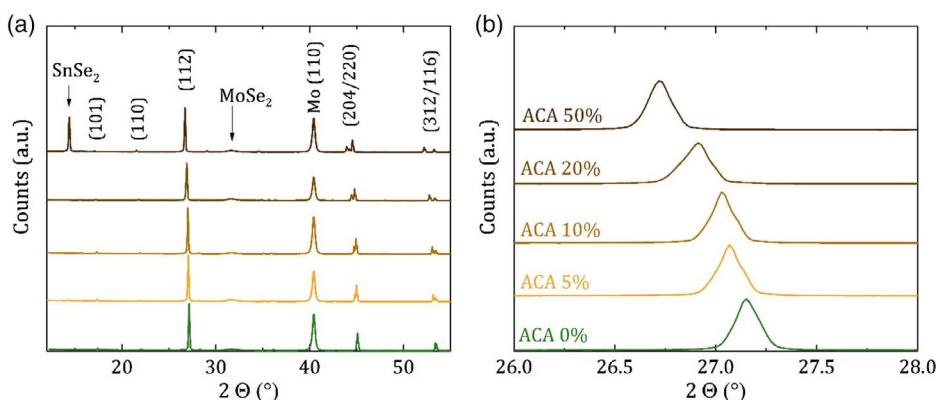


Figure 1. a) XRD patterns for the CAZTSe absorbers with different ACA ratios and b) zoom of the XRD patterns on the (112) diffraction peaks. Same color code for both graphs.

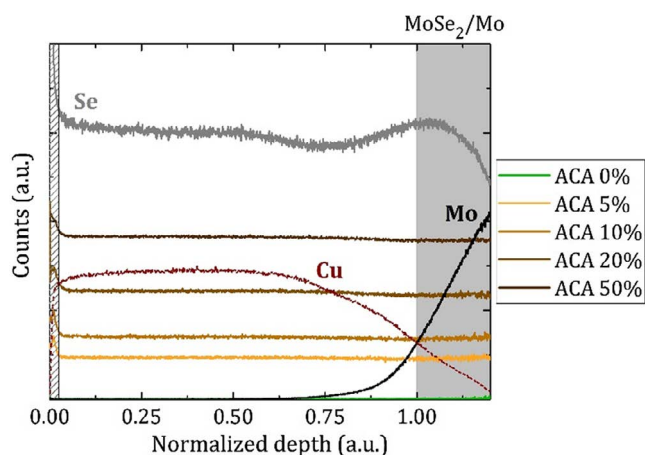


Figure 2. GDOES profiles of the CAZTSe absorbers for different ACA ratios. Cu, Se, and Mo profiles of the Ag 10% sample are shown as well. The MoSe₂/Mo back contact has been arbitrarily placed at the Cu and Mo signal intersection. The hatched area at the surface shows the unreliable zone of plasma stabilization (large variation of the plasma module and phase impedance matching).

synthesized at 500 °C and are very similar. Large (>1 μm) and slightly rounded grains are obtained regardless of the Ag content. Particularly, no material decomposition such as that mentioned in the study by Huang et al.^[7] is observed, even for the ACA 20% and ACA 50%. In the latter case, the presence of small dots on the surface is attributed to the unavoidable presence of SnSe₂.

The use of these homogeneous CAZTSe absorbers in Mo/CATZSe/CdS/i-ZnO/ZnO:Al solar cells is described in Section 2.2.1.

2.1.2. Graded Ag Alloying

A second approach developed in this study consists of producing absorbers with graded (Cu and Ag) alloying, with Ag content

increasing at the interfaces. To clearly discriminate the two approaches, absorbers with graded (Cu and Ag) alloying are named CZTSe:Ag in the following sections.

These absorbers are fabricated by Ag incorporation in standard CZTSe absorbers. In a first step, Cu/Sn/Cu/Zn/Se precursor stacks are annealed at 520 °C in additional Se atmosphere to produce the desired material. The process is exhaustively described in the study by Grenet et al.^[16] No modification of the standard process is brought in this approach, particularly concerning the cationic composition: the thicknesses of the precursor stacks are not modified and are similar to those used in the highly efficient CZTSe technology.^[16] The composition of the CZTSe absorbers is shown in Table 2. After CZTSe synthesis, a Ag thin layer (from 5 to 15 nm) is sputtered on top of the absorber without intentional heating. To force Ag diffusion in the CZTSe layer, a hot plate annealing stage in air is then performed. Temperatures of 200, 300, and 400 °C for 10 min have been tested.

Elemental profiles in the CZTSe:Ag layers have been determined by GDOES. ACA ratios for the Ag 10 nm sample with different hot plate annealing temperatures are shown in Figure 4 along with the ACA ratio for the homogeneous Ag 10% sample. Se and Mo profiles are shown for clarity. This graph shows clearly the interest of this approach: contrary to the CAZTSe absorbers, the CZTSe:Ag materials have an almost null ACA ratio in the bulk but with significant signal increase at both interfaces. The presence of Ag at the front interface can be debated because of the plasma stabilization artifact but is further confirmed by X-ray photoelectron spectrometer (XPS) measurements (Table 3). Surprisingly, the ACA ratios are absolutely not modified by the hot plate annealing stage: indeed, the as-deposited (as dep.) sample (without hot plate annealing) already shows a large ACA ratio at the back interface, meaning that diffusion occurs at room temperature during the Ag sputtering process.

Table 3 shows the ACA ratio measured in the Ag 10 nm sample (same as in Figure 4) with EDX and XPS. EDX measurements have been carried out at 20 keV, for which the integration

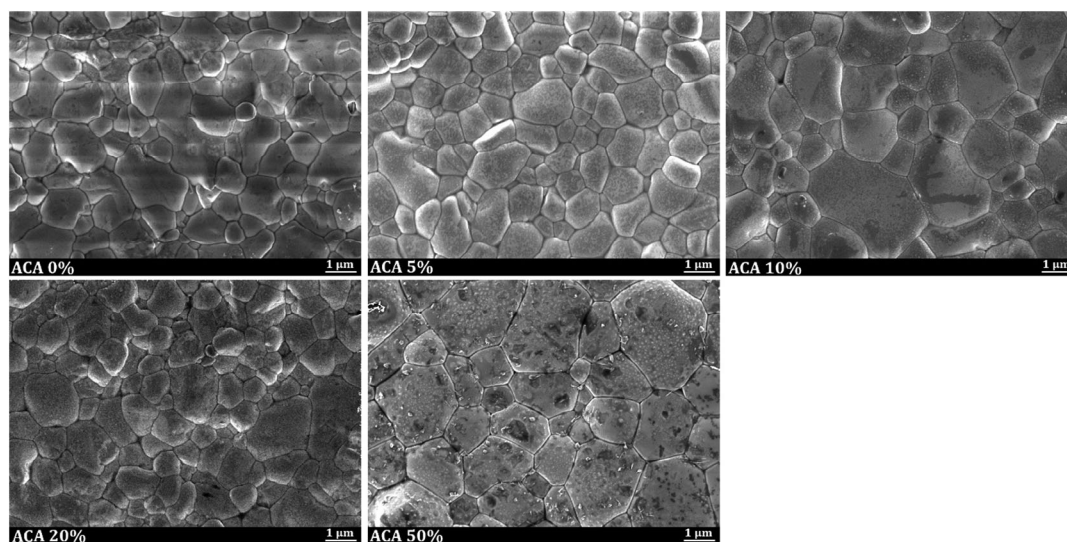


Figure 3. SEM top views of the CAZTSe absorbers for different ACA ratios.

Table 2. Composition of the CZTSe samples used for Ag-graded alloying before Ag diffusion measured by XRF.

Sample	Cu [at%]	Zn [at%]	Sn [at%]
Ag 0 nm	42.8 ± 0.3	29.5 ± 0.3	27.7 ± 0.4
Ag 5 nm	42.9 ± 0.3	29.8 ± 0.3	27.3 ± 0.4
Ag 10 nm	42.9 ± 0.3	29.9 ± 0.3	27.1 ± 0.4
Ag 15 nm	42.9 ± 0.3	29.7 ± 0.3	27.4 ± 0.4

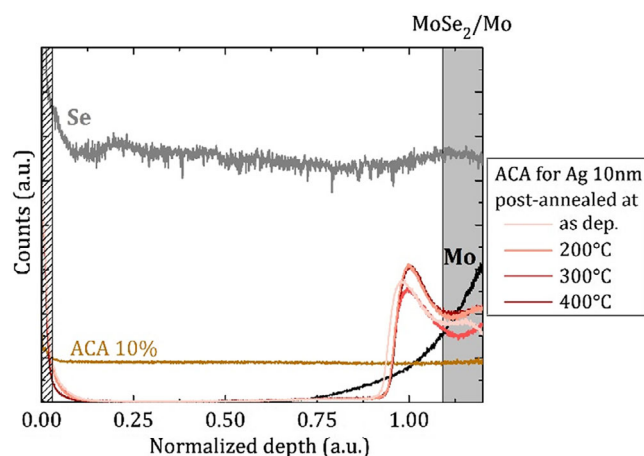


Figure 4. GDOES elemental profiles in the Ag 10 nm sample for different post-annealing temperatures: all curves almost overlap. The ACA 10% profile is added for comparison purpose. The MoSe₂/Mo back contact has been arbitrarily placed at the Cu and Mo signal intersection. The dashed area at the surface shows the unreliable zone of plasma stabilization.

Table 3. ACA ratio for the Ag 10 nm sample after hot plate annealing at various temperatures and measured by EDX at 20 keV and XPS.

T [°C]	ACA [%] – EDX	ACA [%] – XPS
As dep.	3.9	45
200 °C	2.6	–
300 °C	3.3	37
400 °C	0.9	–

sphere is similar to the layer thickness (the contribution of the Mo back contact is negligible). These values are not significant and cannot be compared with Table 1 as the distribution of Ag is totally not homogeneous in the sample. However, they show that the amount of Ag in the CZTSe:Ag layers is not negligible before and after the hot plate annealing stage. XPS measurements (Figure S1, Supporting Information) have been carried out to confirm the presence of Ag at the very surface of the absorber. First, ACA ratio for the as-deposited sample reveals that the surface does not only consist of a thin Ag layer but is already made of CAZTSe. Only a slight decrease in the ACA ratio is observed with the hot plate annealing stage (Table 3). In addition, XPS spectra focused on Ag 3d peaks (Figure S1, Supporting

Information) do not show any shift in the peak position, confirming that most of the Ag present at the surface is in the form of CAZTSe alloy even before annealing.

Further insight into the CZTSe:Ag layers is given with the EDX cross section shown in Figure 5 for the Ag 10 nm sample. The first, second, and third columns show the Ag, Cu, and Mo signals, respectively. On the second line the Ag 10 nm sample is shown without hot plate annealing, whereas the third, fourth, and fifth lines, respectively, exhibit the sample with 200, 300, and 400 °C hot plate annealing stages. The first line shows the homogeneous ACA 10% sample for comparison. In this case, the Ag signal is relatively well overlapped to the Cu signal and above the Mo one. On the contrary, for the CZTSe:Ag sample depicted in all other lines, the Ag signal is mainly visible at the absorber interfaces. A weak (sometimes hardly discernible) but continuous Ag signal is always visible close to the back interface, whereas additional bright Ag spots (Ag particles) are equally visible at both interfaces (front surface and absorber/back contact interface). In the Ag 10 nm sample post-annealed at 300 °C, an Ag spot is even visible within the absorber.

The integration of the CZTSe:Ag absorbers in Mo/CZTSe:Ag/CdS/i-ZnO/ZnO:Al solar cells is described in Section 2.2.2.

2.2. Integration in Devices

2.2.1. Homogeneous Alloying

CAZTSe absorbers have been used in Mo/CAZTSe/CdS/i-ZnO/ZnO:Al solar cells. A vast amount of process parameters have been tested to synthesize the CAZTSe absorbers (Ag below or above the Cu/Sn/Cu/Zn stack, synthesis temperature varying from 400 to 500 °C, variation in the cationic Cu + Ag, Zn, and Sn composition). PCEs of all these devices are shown as a function of their ACA ratio in Figure 6a, regardless of the synthesis process. This representation has been chosen to evidence that the incorporation of Ag is not beneficial for kesterite devices despite numerous attempts to optimize the performances of CAZTSe-based solar cells. At first sight, this result is in contradiction with numerous previous studies^[6–13] in which an optimum is found at low (but not null) ACA ratios. All the literature data concerning Ag alloying for kesterite solar cells have been shown in Figure 6b along with the state-of-the-art PCE for sulfur, selenium, and sulfoselenium Ag-free absorbers. With this representation, the beneficial effect of Ag alloying is more subject to discussion, whether it is a fundamental effect or the result (in each publication) of a specific process optimization centered at low Ag content: indeed, it can be noticed that in each study, limited efficiencies are obtained for the reference Ag-free device (between 3% and 9%). In addition, numerous studies have been published for CAZTSSe devices and no particular ACA ratio optimum can be evidenced (variation from 3% to 20%).

J–V curves of CAZTSe-based solar cells with increasing ACA ratios (from 0% to ≈50%) are shown in Figure 7a. All PV properties (fill factor [FF], open-circuit voltage V_{OC} , and short-circuit current J_{SC}) decrease with increasing ACA ratio and no V_{OC} gain is observed though smaller band tails are expected. External quantum efficiency (EQE) spectra of the same solar cells are shown in Figure 7b. The shapes of the spectra are not affected

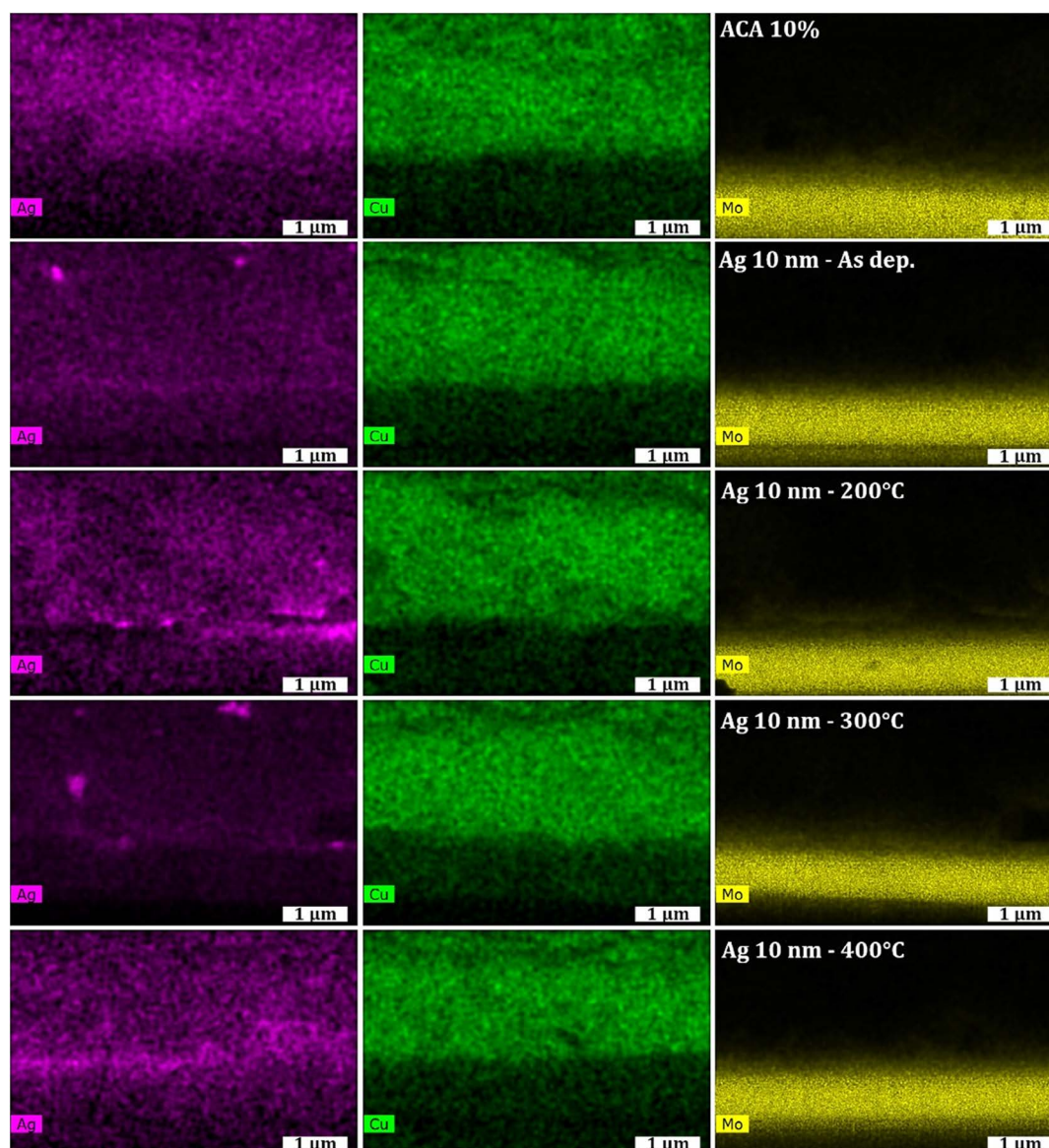


Figure 5. EDX mappings (Ag in violet, Cu in green, and Mo in yellow) for the ACA 10% sample (first line) and the Ag 10 nm sample with different post-annealing temperatures.

by Ag incorporation but the maximum value is strongly reduced (Table S1, Supporting Information), and the bandgap is shifted to higher energies. The low EQE at all wavelengths can originate from high series resistance, low doping (along with a limited lifetime), or a potential barrier at the absorber/buffer interface.^[20] The bandgap extracted from the maximum of the EQE first derivative is shown in Figure 7c. It increases linearly with the Ag content; the absence of bowing confirms the well-defined $(\text{Cu}_{1-x}\text{Ag}_x)_2\text{ZnSnSe}_4$ alloy solid solution. A decrease in p-type conductivity (and shift to n-type conductivity for $\text{ACA} > 50\%$)^[9] can be claimed to be responsible for the efficiency drop in CAZTSe/CdS/ZnO:Al solar cells at a high ACA ratio. $C-V$ measurements carried out at room temperature reveal a one order of magnitude decrease in the apparent free carrier concentration for ACA varying from 0% to 50%. This reduction cannot explain the

poor performances at high Ag content. According to the set of characterizations shown in Figure 7, a detrimental interface or band alignment is more likely to explain the low CAZTSe-based solar cells performances.

2.2.2. Graded Alloying

In a second part, CZTSe:Ag absorbers have been used in the same solar cell structures. The PCEs of Ag 5 nm, Ag 10 nm, and Ag 15 nm are shown in Figure 8a as a function of the hot plate annealing temperature. For clarity, only the best cell PCE is shown in Figure 8 but the results from all cells are depicted in terms of box plots in Figure S2, Supporting Information.

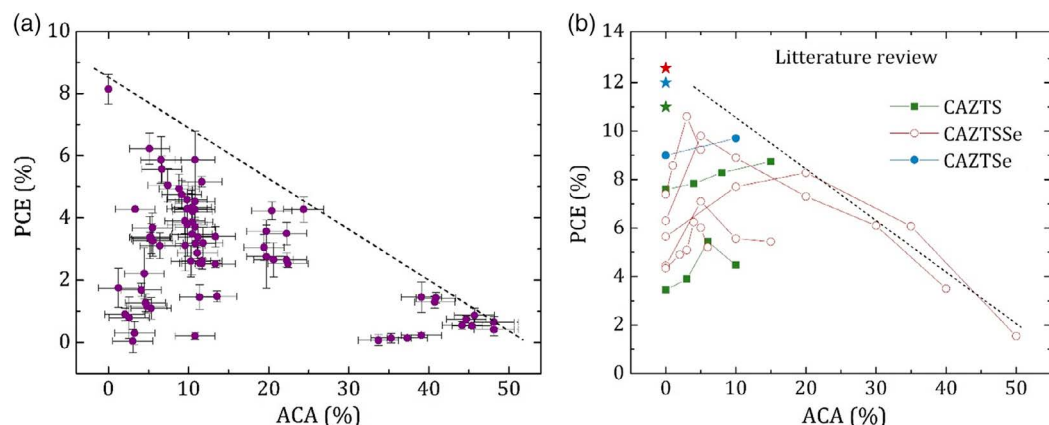


Figure 6. a) PCE of the CAZTSe-based solar cells as a function of the ACA ratio. Each point represents the median PCE over at least nine cells for each sample. A mean 2.5% x-error bar (from EDX uncertainty) has been applied to all samples; the y-error bar is the difference between the maximum and median values for each sample. The dashed line is a guide for the eye. b) Literature review of the maximum PCE for CAZTS(S)(e) as a function of the ACA ratio.^[6–13] Stars represent the state-of-the-art efficiency for CZTS, CZTSSe, and CZTSe solar cells respectively.^[17–19] The dashed line is a guide for the eye.

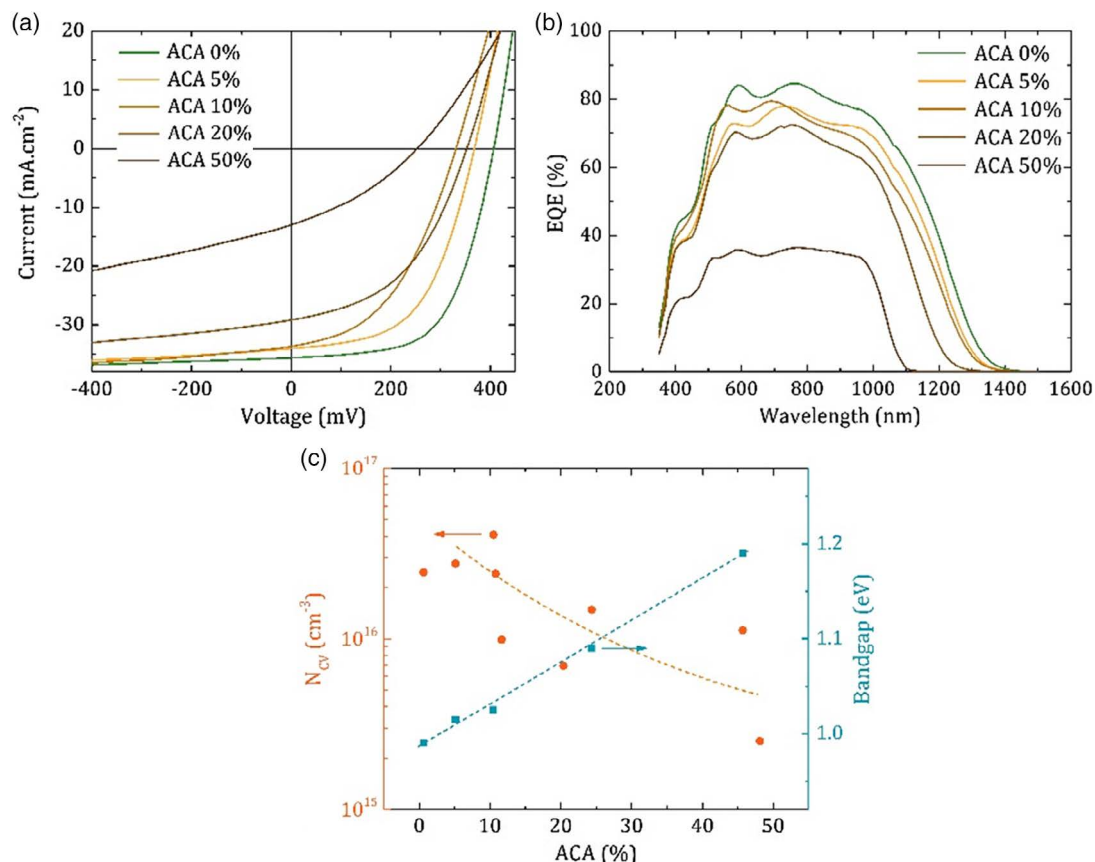


Figure 7. a) J - V curves of selected solar cells with various ACA ratios. b) EQE spectra of the same CAZTSe-based solar. c) Apparent free carrier concentration (N_{cv}) (left scale in orange) and bandgap (right scale in blue) of the CAZTSe absorbers as a function of the ACA ratio.

As it is well-known that CZTSe absorbers are improved by air annealing prior to CdS deposition,^[21,22] the PCE of the pure CZTSe solar cell (Ag 0 nm) is depicted as well. The PCE of CZTSe:Ag-based solar cells shows a very narrow air-annealing temperature optimum compared with the Ag-free device. In the

CZTSe case, reasonable efficiencies are obtained in a 200–300 °C range of temperature, whereas for CZTSe:Ag samples, good performances are only achieved at 300 °C. At this temperature, Ag 5 nm and Ag 10 nm exhibit PCEs comparable and even better in the latter case than the reference Ag 0 nm sample. The lower

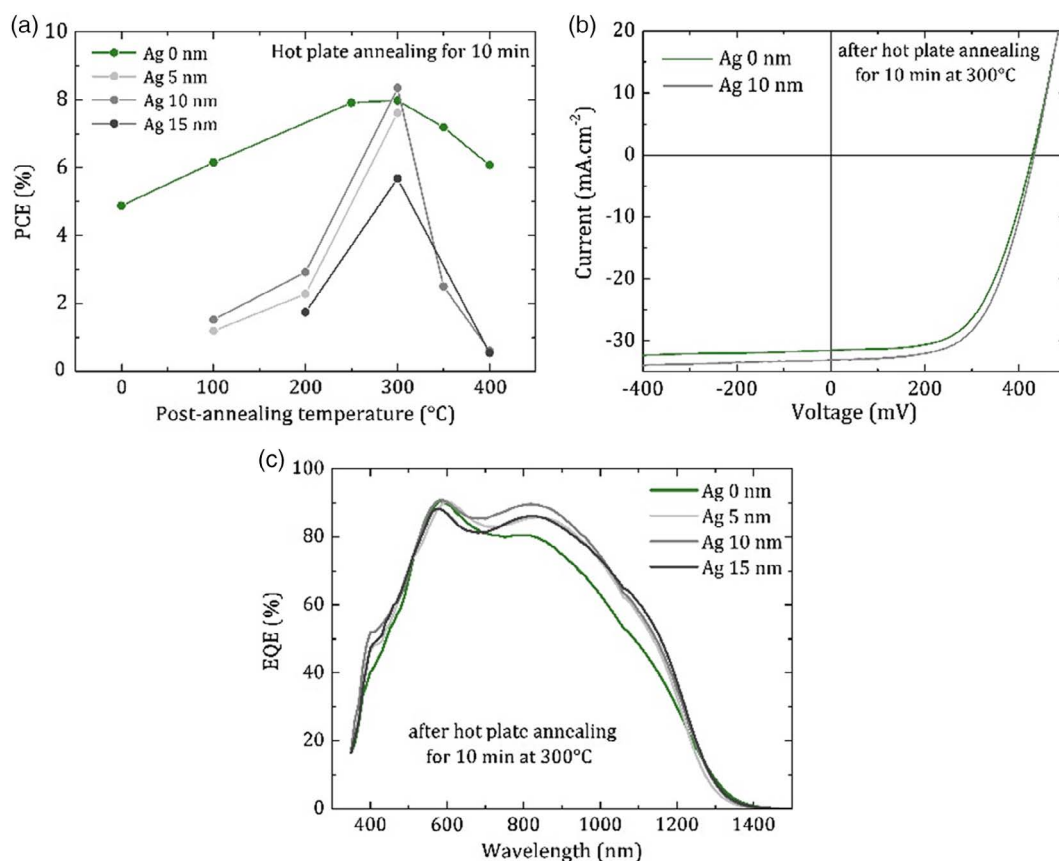


Figure 8. a) PCE of the solar cells with Ag post-diffusion for different Ag thicknesses and as a function of the post-annealing temperature. b) J - V curves of the best CZTSe and CZTSe:Ag after hot plate annealing at 300 °C for 10 min. c) EQE spectra of the CZTSe and CZTSe:Ag solar cells after 10 min—300 °C post-annealing.

PCE in the case of Ag 15 nm is attributed to a too important Ag incorporation in the sample (the $(\text{Cu} + \text{Ag})/(\text{Zn} + \text{Sn})$ ratio becomes too large). Improvement in the PCE for the CZTSe:Ag-based solar cell is mainly attributed to a larger J_{SC} , as clearly visible in the J - V curve shown in Figure 8b. EQE spectra (Figure 8c) confirm the larger J_{SC} for CZTSe:Ag-based devices and explicit the long wavelength improvement of the EQE, which is attributed to a better carrier collection at the back of the absorber. Values of the integrated photon current density are shown in Table S2, Supporting Information. The improved carrier collection at the Mo/absorber interface in case of the graded ACA ratio toward the back interface has already been observed.^[6] A small EQE improvement at short wavelengths can also be noticed. As similar CdS thicknesses are used for all samples, the higher EQE can be attributed to reduced interface recombination, as shown in the study by Suzon et al.^[23] The small amount of Ag at the surface improves as well the CZTSe:Ag/CdS interface.

3. Conclusions

This study demonstrates the possibility of synthesizing $(\text{Cu}_{1-x}\text{Ag}_x)_2\text{ZnSnSe}_4$ absorbers with homogeneous and graded alloying profiles by vacuum processes. In the first case, perfect solid solutions are obtained in the depth of the absorber for

Ag content up to 50%. These CAZTSe absorbers reveal good morphologies with large grains and without evidence of secondary phases except for the highest Ag content. However, and contrary to most of the published literatures, homogeneous incorporation of Ag in kesterite absorbers does not lead to better performances of the PV devices. A careful literature review shows that the performances of the best Ag-substituted CAZTSe(e) devices are still lower than the state-of-the-art Ag-free CZTSe(e) ones. Thus, the PCE value of the reference solar cell is a critical parameter to claim for a beneficial effect of cationic substitution (with Ag, Cd, Mg, Ge, and so on) in the kesterite matrix.

On the other hand, a very innovative method has been developed to fabricate CAZTSe absorbers with graded Ag content. A significant ACA ratio increase close to the back and front interfaces has been demonstrated by different methods. Particularly, the presence of a Ag-rich $(\text{Cu}_{1-x}\text{Ag}_x)_2\text{ZnSnSe}_4$ layer close to the Mo back contact helps to collect the carrier at this interface and improve current in the devices. A slight reduction of the absorber/buffer recombination is shown as well.

The post-treatment method used to fabricate Ag-graded absorbers is easily implementable in a process line and can be tested by others groups without modifying the baseline process. It allows to optimize the solar cell performances with very limited amounts of Ag by limiting the losses at the interfaces.

4. Experimental Section

Received: January 28, 2020

Revised: February 18, 2020

Published online:

Samples Preparation: CZTSe absorbers were synthesized in a two-step selenization process. Cu/Sn/Cu/Zn precursors were sputtered in an Alliance Concept equipment onto a Mo-coated soda-lime glass substrate. The samples were positioned in a graphite susceptor with Se pellets and annealed at 520 °C for 5 min at 8.5×10^4 Pa Ar pressure in a lamp furnace. Additional details of the CZTSe absorber fabrication were shown in the study by Grenet et al.^[16]. Ag was deposited in an Alliance Concept DPI100 equipment with high-power impulse magnetron sputtering.

The solar cells were completed with a 70 nm CdS buffer layer deposited by a chemical bath. Cadmium acetate (1×10^{-3} M), thiourea (5.1×10^{-3} M), ammonium acetate (20×10^{-3} M), and ammonia (0.3×10^{-3} M) were stirred at 600 rpm, and the samples were immersed in the solution at 80 °C for 15 min. A 50 nm/250 nm i-ZnO/ZnO:Al (Al₂O₃ 2 at%) window layer was radio frequency (RF) sputtered in an MRC2 chamber without intentional sample heating. Ni (50 nm)/Al (500 nm) grids were thermally evaporated on top of the solar cell. At least ten 0.5×0.5 cm² solar cells were manually scribed on each sample. No antireflecting coating was used in this study.

Characterization: XRD diffractograms were acquired in a D8 Advance Bruker AXS with a copper counter electrode X-ray tube. SEM images and energy-dispersive spectroscopy (EDS) measurements were carried out in a Zeiss LEO 1530 equipment. The compositions of the CZTSe layers were determined by XRF in a FISCHERSCOPE X-RAY XDV-SDD equipment working at 50 kV. Elemental profiles in the absorber were measured by GDOES in a Horiba Profiler II equipment.

A Spectra-Nova's CT Series Solar Cell Tester was used to carry out current–voltage (J–V) measurements under simulated AM1.5G spectrum (100 mW cm^{-2}). Solar spectrum of the simulator was calibrated prior all measurements with a calibrated crystalline Si device. All J–V measurements (light and dark) were carried out at 25 °C in a four-point probe configuration. EQE measurements were carried out in a ReRa Spequest spectrometer. Capacitance–voltage (C–V) measurements were carried out at 110 kHz and at room temperature with a 50 mV oscillating voltage in an Agilent HP E4980A Precision LCR meter. XPS analyses were conducted on a PHI Versaprobe II spectrometer using a monochromated Al K α (1486.7 eV) X-ray beam.

Supporting Information

Supporting Information is available from the Wiley Online Library or from the author.

Acknowledgements

This research was supported by the H2020 Program under the project STARCELL (H2020-NMBP-03-2016-720907) and the ANR Carnot Energies du Futur program under the project CAZTS. The authors thank Eric De Vito for the XPS measurements.

Conflict of Interest

The authors declare no conflict of interest.

Keywords

Ag alloying, graded bandgaps, homogeneous alloying, kesterite, thin film photovoltaics

- [1] M. A. Green, Y. Hishikawa, E. D. Dunlop, D. H. Levi, J. Hohl-Ebinger, M. Yoshita, A. W. Y. Ho-Baillie, *Prog. Photovoltaics* **2019**, 27, 3.
- [2] L. Grenet, M. A. A. Suzon, F. Emieux, F. Roux, *ACS Appl. Energy Mater.* **2018**, 1, 2103.
- [3] S. Nakamura, T. Maeda, T. Tabata, T. Wada, in *Proc. 37th IEEE Photovoltaic Specialists Conf.*, IEEE, Piscataway, NJ **2011**, pp. 002771–002774.
- [4] Z. K. Yuan, S. Chen, H. Xiang, X. G. Gong, A. Walsh, J. S. Park, I. Repins, S. H. Wei, *Adv. Funct. Mater.* **2015**, 25, 6733.
- [5] H. Cui, X. Liu, F. Liu, X. Hao, N. Song, C. Yan, *Appl. Phys. Lett.* **2014**, 104, 041115.
- [6] Y.-F. Qi, D.-X. Kou, W.-H. Zhou, Z.-J. Zhou, Q.-W. Tian, Y.-N. Meng, X.-S. Liu, Z.-L. Du, S.-X. Wu, *Energy Environ. Sci.* **2017**, 10, 2401.
- [7] W.-C. Huang, S.-Y. Wei, C.-H. Cai, W.-H. Ho, C.-H. Lai, *J. Mater. Chem. A* **2018**, 6, 15170.
- [8] C. Yan, J. Huang, K. Sun, Y. Zhang, M. A. Green, X. Hao, in *Proc. IEEE 7th World Conf. on Photovoltaic Energy Conversion (WCPEC)*, IEEE, Piscataway, NJ **2018**, pp. 3709–3711.
- [9] T. Gershon, Y. S. Lee, P. Antunez, R. Mankad, S. Singh, D. Bishop, O. Gunawan, M. Hopstaken, R. Haight, *Adv. Energy Mater.* **2016**, 6, 1502468.
- [10] Y. Qi, Q. Tian, Y. Meng, D. Kou, Z. Zhou, W. Zhou, S. Wu, *ACS Appl. Mater. Interfaces* **2017**, 9, 21243.
- [11] M. H. Sayed, J. Schoneberg, J. Parisi, L. Guetay, *Mater. Sci. Semicond. Process.* **2018**, 76, 31.
- [12] S. Yang, S. Wang, H. Liao, X. Xu, Z. Tang, X. Li, T. Wang, X. Li, D. Liu, *J. Mater. Sci.: Mater. Electron.* **2019**, 30, 11171.
- [13] X. Yu, S. Cheng, Q. Yan, J. Yu, W. Qiu, Z. Zhou, Q. Zheng, S. Wu, *RSC Adv.* **2018**, 8, 27686.
- [14] C. Platzer-Björkman, N. Barreau, M. Bär, L. Choubrac, L. Grenet, J. Heo, T. Kubart, A. Mittiga, Y. Sanchez, J. Scragg, *J. Phys.: Energy* **2019**, 1, 044005.
- [15] D. Bishop, T. Gershon, Y. S. Lee, P. Antunez, R. Mankad, S. Singh, O. Gunawan, R. Haight, in *Proc. IEEE 43rd Photovoltaic Specialists Conf. (PVSC)*, IEEE, Piscataway, NJ **2016**, pp. 0173–0178.
- [16] L. Grenet, M. A. A. Suzon, F. Emieux, F. Roux, *J. Renewable Sustainable Energy* **2018**, 10, 043503.
- [17] W. Wang, M. T. Winkler, O. Gunawan, T. Gokmen, T. K. Todorov, Y. Zhu, D. B. Mitzi, *Adv. Energy Mater.* **2014**, 4, 1301465.
- [18] C. Yan, J. Huang, K. Sun, S. Johnston, Y. Zhang, H. Sun, A. Pu, M. He, F. Liu, K. Eder, *Nat. Energy* **2018**, 3, 764.
- [19] X. Li, D. Zhuang, N. Zhang, M. Zhao, X. Yu, P. Liu, Y. Wei, G. Ren, *J. Mater. Chem. A* **2019**, 7, 9948.
- [20] R. Scheer, H.-W. Schock, *Chalcogenide Photovoltaics: Physics, Technologies, and Thin Film Devices*, Wiley, Weinheim, Germany **2011**, p. 312.
- [21] M. Neuschitzer, Y. Sanchez, T. Olar, T. Thersleff, S. Lopez-Marino, F. Oliva, M. Espindola-Rodriguez, H. Xie, M. Placidi, V. Izquierdo-Roca, *Chem. Mater.* **2015**, 27, 5279.
- [22] L. Grenet, F. Emieux, E. De Vito, F. Roux, To be published **2019**.
- [23] M. A. A. Suzon, L. Grenet, F. Emieux, E. De Vito, F. Roux, H. Mariette, *Phys. Status Solidi A* **2019**, 216, 1900070.